DATA-WORTH ANALYSIS: DESIGNING A MONITORING PLAN FOR ROTORUA THAT REDUCES UNCERTAINTY

Ken Dekkers[1], Michael Gravatt[1], Oliver J. Maclaren[1], Ruanui Nicholson[1], John O'Sullivan[1], Michael O'Sullivan[1]

[1] Department of Engineering Science, University of Auckland, 70 Symonds Street, Grafton, Auckland 1010, New Zealand

jp.osullivan@auckland.ac.nz

Keywords: *Reservoir modelling, Rotorua, Uncertainty quantification, Data-worth analysis*

ABSTRACT

Developing an accurate geothermal model requires model calibration to match available data. The data is expensive to gather and, therefore, usually sparse. It is common to use geothermal models to make predictions that aid in managing the geothermal field sustainably. However, these model predictions are uncertain due to model complexity and sparse data. This paper discusses how we can quantify that uncertainty and how we can design monitoring plans to reduce the uncertainty in model predictions in the context of the Rotorua geothermal field. The design of monitoring plans for uncertainty reduction falls under the area of data-worth analysis.

From 1950 to 1986, the state of the reservoir of Rotorua was deteriorating. Therefore, the government and the Bay of Plenty Regional Council collected valuable monitoring data that helps to sustainably manage the geothermal field. There are many individual users of the geothermal reservoir, and it is not known exactly how much production has occurred in the past from various users. Uncertainty in production rates is an unusual situation compared to other geothermal reservoirs, as usually the production and reinjection are known. We have hence developed a new geothermal model for Rotorua that considers the uncertainty in production and reinjection. Using the new model, we can make model predictions that have uncertainty bands that provide better information for reservoir management.

In this paper, we consider uncertainty and data-worth analyses for Rotorua using our new model. We present three scenarios of monitoring plans for taking additional measurements in Rotorua and compare how measuring new data in different locations reduces the uncertainty in model predictions. The results of these monitoring scenarios show the benefit of data-worth analysis using simulation models: we can assess the possible effect of new monitoring plans before spending any money on these further measurements.

1. INTRODUCTION

1.1 Rotorua geothermal field

Under the township of Rotorua there is a large source of geothermal energy. The geothermal activity of the Rotorua geothermal field (RGF) is due to its location in the Taupō Volcanic Zone. Long before any wells were drilled into the geothermal reservoir, the geothermal heat of the reservoir was used for bathing and cooking by Māori. Since 1950 the reservoir was further utilised by means of production wells. However, unregulated production was not sustainable and geothermal surface features of the reservoir started to decline. This led to a wellbore closure programme in 1986, which meant that no production was allowed within a 1.5km radius of the Pohutu Geyser and 90% of the production had to be reinjected (Environment Bay of Plenty (EBOP), 1999). A map of the RGF with the wells before and after the Wellbore Closure Programme, the Exclusion Zone and geothermally active surface areas is shown in Figure 1.

Generally, the development of geothermal reservoirs is managed by a small number of (commercial) users. Usually there are detailed records of the production rates as well as temperature and pressure measurements at various depths of the reservoir. However, in the case of Rotorua there are many individual users with sparse (or non-existent) production records, and only shallow temperature measurements are available. The lack of production records and deep measurements make it difficult to develop an accurate model.

1.2 Numerical model

We have recently developed an improved numerical model for Rotorua, UOA Model 5, at The University of Auckland (UOA) (Dekkers, et al., 2020). The main improvements in this model compared to our previous model, UOA Model 4a, are:

- A higher numerical accuracy due to mesh refinement and hence more blocks (94,701 vs 48,034).
- A change in grid type (regular rectangular in this case) allowing AUTOUGH2 and Waiwera to be used on this model. In this paper we discuss results obtained with Waiwera (Croucher, et al., 2020) because of its faster computation time and easy access to the model sensitivity matrix (used for uncertainty quantification).
- The new fault structure is a more accurate representation of the geology.
- A clay cap has been implemented by using new rock types in the model. This allows more heterogeneity to better represent the geothermal flows.

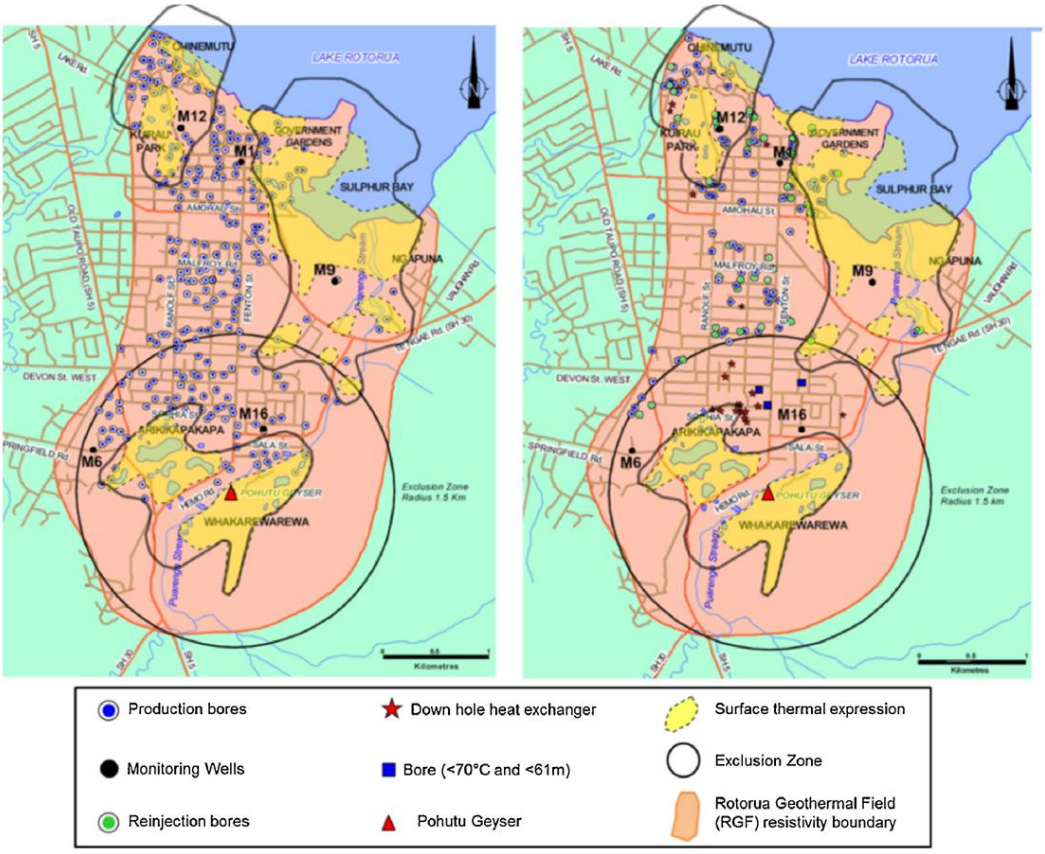

Figure 1: A map of Rotorua geothermal field with all wells before (left) and after (right) the Wellbore Closure Programme in 1986. The Exclusion Zone and geothermally active surface areas are indicated as well. (Ratouis, O'Sullivan, & O'Sullivan, 2016).

1.3 Model uncertainty

Even though improving the numerical model will improve the accuracy of the model predictions, a numerical model will always be an approximation of reality and thus contain uncertainty. This is due to errors made in the modelling process, measurement errors, sparsity of the field data and numerical accuracy. Therefore, quantifying the uncertainty of model predictions is desirable and provides more informative predictions than using a single best estimate model only.

In our new numerical model for Rotorua, we have included the uncertainty of the model parameters, including permeability, deep upflow source rates, and production and reinjection rates. The analysis of the uncertainty of the model predictions is described by Dekkers (2021).

In this paper we focus on how we can reduce the uncertainty of model predictions by a data-worth analysis (DWA). We estimate the effect of new measurements by designing potential monitoring plans. As monitoring a geothermal field is expensive, gaining insight about the best places to measure data is valuable.

2. METHODOLOGY

We consider uncertainty quantification (UQ) and data-worth analysis in the Bayesian framework (Kaipio & Somersalo, 2006), as it naturally allows for incorporation and quantification of various sources and types of uncertainty. Here we briefly recall the key elements of the Bayesian approach to UQ and DWA. For a more in-depth discussion see, for example, (Alexanderian, 2021) and the references therein.

The most common application of Bayesian UQ in the geothermal context is model calibration (Finsterle, 2007; Cui, Fox, & O'Sullivan, 2011; Maclaren et al., 2020) in which the goal is to estimate (for example) subsurface parameters such as the permeability and deep upflows and quantify their associated uncertainties based on field data such as down-well temperatures. In such cases the typical relationship between the parameters and data is taken to be of the form

$$y = f(p) + e,$$

where $y \in \mathbb{R}^d$ is the data, $p \in \mathbb{R}^n$ denotes the unknown parameters, f represents the forward model, and $e \in \mathbb{R}^d$ the measurement and model error. Assuming *a priori* that the parameters and errors are normally distributed, it is well understood

that the *maximum a priori* (MAP) estimate, i.e., the point in parameter space which maximises the posterior density, is given by

$$p_{\text{MAP}} = \arg\min_{p\in\mathbb{R}^n}\left\{\|y - f(p)\|^2_{C_{obs}^{-1}} + \|p - p_0\|^2_{C_p^{-1}}\right\},$$

where $e \sim \mathcal{N}(0, C_{obs})$ and $p \sim \mathcal{N}(p_0, C_p)$ *a priori*. Quantifying the uncertainty in the parameter estimates is typically done by taking a local Gaussian approximation to the posterior based on linearisation of the forward problem. This results in an approximate posterior of the form $\mathcal{N}(p_{\text{MAP}}, C_{post})$, where

$$C_{post} = \left(S^T C_{obs}^{-1} S + C_p^{-1}\right)^{-1},$$

with S denoting the sensitivity (Jacobian) matrix of the model with respect to the parameters, i.e., $S_{ij} = \partial f_i/\partial p_j$ for $i = 1,2,\dots,d$ and $j = 1,2,\dots,n$.

The general goal of DWA is to measure and compare the value of taking (a set of) new measurements. The value of any new measurement is typically equated with certainty gained, i.e., a larger reduction in uncertainty is valued more. It is worth pointing out that DWA can also be seen as a form of optimal experimental design (OED) (Alexanderian, 2021) or design of experiments (DOE) (Pukelsheim, 2006). Then, if the aim is to minimise the uncertainty in the calibration parameters it is common to seek a new measurement scenario which minimises some measure of C_{post}. The most common optimality criteria are the so-called A-optimality and D-optimality, which are associated with minimising the trace and determinant of C_{post}, respectively (Alexanderian, 2021).

For the management of geothermal reservoirs, it is often the uncertainty in the predictions of various quantities of interest (QOI) (rather than the uncertainty in the parameters) which is the main focus. For example, a reservoir engineer is more interested in predictions of future steam flow from production wells than rock properties at depth. Quantifying the uncertainty in predictions can be accomplished by taking samples from the (approximate) parameter posterior, generating sample models and simulating these to evaluate the QOI. However, this can easily become computationally infeasible in the geothermal context as the forward simulations are computationally expensive and may need to be run for each different data collection scenario. Instead, we propose the use of an essentially linear method which is closely related to the data-space inversion (DSI) methodology (Sun & Durlofsky, 2017; Jiang, Sun, & Durlofsky, 2019).

The proposed approach relies on the key insight that second order uncertainty, i.e., covariance, is independent of data through linear propagation. That is, if the new data $\hat{y}$, and QOI $q \in \mathbb{R}^s$, are related through

$$q = A\hat{y} + \epsilon,$$

then the conditional covariance of q given $\hat{y}$ is given by

$$C_{q|\hat{y}} = C_\epsilon,$$

independent of what the actual new data could be or is. Typically, the mapping A and covariance matrix C_ϵ are unknown *a priori*. However, these can be approximated using samples, and importantly, for all the new measurement scenarios simultaneously. More specifically, an ensemble of samples, say $p^{(i)}$ for $i = 1,2,\dots,E$, are generated from the (approximate) parameter posterior and are run through to each of the proposed new data collection scenarios as well as to the QOI, giving a new ensemble of $\left(q^{(i)}, \hat{y}_1^{(i)}, \hat{y}_2^{(i)}, \dots, \hat{y}_M^{(i)}\right)$, where each of the $\hat{y}_j^{(i)}$ for $j = 1,2,\dots,M$ are the M proposed new measurement scenarios. From this ensemble we can compute the sample covariance matrix,

$$\tilde{C}_{q\hat{y}} = \frac{1}{E-1}\mathcal{C}\mathcal{C}^T = \begin{bmatrix} \tilde{C}_q & \tilde{C}_{q\hat{y}_1} & \dots & \tilde{C}_{q\hat{y}_M} \\ \tilde{C}_{\hat{y}_1 q} & \tilde{C}_{\hat{y}_1} & \dots & \tilde{C}_{\hat{y}_1\hat{y}_M} \\ \vdots & \vdots & \ddots & \vdots \\ \tilde{C}_{\hat{y}_M q} & \tilde{C}_{\hat{y}_M\hat{y}_1} & \dots & \tilde{C}_{\hat{y}_M} \end{bmatrix},$$

where $\mathcal{C}(:,j) = \left(q^{(j)}, \hat{y}_1^{(j)}, \hat{y}_2^{(j)}, \dots, \hat{y}_M^{(j)}\right)^T - \left(\tilde{q}, \tilde{\hat{y}}_1, \tilde{\hat{y}}_2, \dots, \tilde{\hat{y}}_{\text{M}}\right)^T$, with the sample means given by

$$\tilde{q} = \frac{1}{E}\sum_{k=1}^{E} q^{(k)}, \qquad \tilde{\hat{y}}_1 = \frac{1}{E}\sum_{k=1}^{E} \hat{y}_1^{(k)}, \qquad \tilde{\hat{y}}_2 = \frac{1}{E}\sum_{k=1}^{E} \hat{y}_2^{(k)}, \qquad \dots, \qquad \tilde{\hat{y}}_{\text{M}} = \frac{1}{E}\sum_{k=1}^{E} \hat{y}_M^{(k)}.$$

The conditional covariance $C_{q|\hat{y}_i}$, i.e., the covariance of the QOI conditioned on carrying out measurement scenario $\hat{y}_i$, can then be computed as

$$C_{q|\hat{y}_i} = \tilde{C}_q - \tilde{C}_{q\hat{y}_i}\tilde{C}_{\hat{y}_i}^{-1}\tilde{C}_{\hat{y}_i q}, \qquad \text{for } i = 1,2,\dots,M.$$

The optimal data collection strategy is then the strategy which minimises the optimality criteria applied to $C_{q|\hat{y}_i}$.

3. MODEL SETUP

3.1 Numerical model

Modelling a geothermal reservoir starts by simulating the natural state, or steady state, of the reservoir. The next step is to include production and reinjection and simulate the production history. In this study, the production history model is extended to 2041 to forecast the future state of the RGF reservoir. In a previous study, natural state samples were generated using an uncertainty distribution on the log-permeability values and the deep upflow rates with standard deviations of log(0.25) and μ/10, respectively, where μ is the calibrated upflow rate. Using the New Zealand eScience Infrastructure (NeSI) (NIWA, the University of Acukland, University of Otago, Manaaki Whenua - Land Research, 2021) a total of 826 natural state sample models were simulated, and 279 sample models converged to a steady state solution. The uncertainty quantification of these simulations can be seen in the work of (Dekkers, 2021).

We used the results of the natural state sample models as an input for the production history models. Furthermore, an uncertainty on the production and reinjection rates was applied. The production uncertainty used in this paper differs from the work of (Dekkers, 2021). In this paper we used a skew-normal distribution, instead of a normal distribution, for the production and reinjection rates to increase the likelihood of the production being higher than the estimates. The probability density function is of the form,

$$h(x) = \frac{2}{\omega}\varphi\left(\frac{x-\xi}{\omega}\right)\theta\left(\alpha\frac{x-\xi}{\omega}\right),$$

with the skewness scale ω = 0.4, the location $\xi = 0.9$ and the shape α = 10. The functions φ and θ represent the standard normal density function and its cumulative distribution function, respectively. Furthermore, a time-dependent correlation has been used of the form,

$$\{R_{\text{flowrate}}\}_{\text{ij}} = e^{-\frac{(t_i - t_j)^2}{2l^2}},$$

where l is the characteristic timescale set to 200 and t_i and t_j are points in time. An illustration of the production distribution of a single well and the sum of the wells is shown in Figure 2.

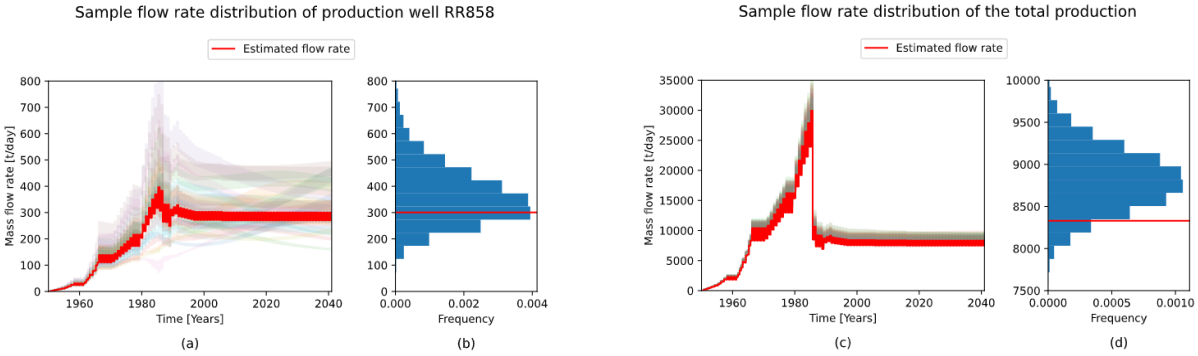

Figure 2: In (a) and (c) we see the distribution of the sample production rates of a single production well RR858 (a) and the sum of the production wells (c), where the red fluctuating line indicates the estimated seasonal production rates and the semitransparent colored lines indicate the generated sample production rates. In (b) and (d) the blue histograms show the production rate distribution in 2041 for well RR858 (b) and the sum of all production wells (d), the red line indicates the estimated production rate in 2041.

The skewed normal distribution was applied on all production and reinjection flow rates. The output of the natural state sample models and the uncertain production rates were used to generate production history sample models. The reinjection wells are linked to production wells, which means the reinjection rates vary for each sample and for each region the reinjection is still 90% of the production. In total 279 production history sample models were simulated using NeSI and the results were used for the DWA.

3.2 Monitoring scenarios

In this paper we analyse the temperature, pressure and mass outflow (QOI). The production history sample results show the prediction uncertainty in our QOI caused by uncertain model parameters. For this paper we compare the impact of three different monitoring scenarios on the uncertainty of our model predictions using a DWA. For the implementation of the DWA we used the Python package *ccandu* (‘conditional composition and uncertainty quantification’) currently in development by the ‘Modelling Uncertainty and Data’ group at the University of Auckland (Modelling Uncertainty and Data Group UoA, 2021). The *ccandu* package is based on Gaussian approximations. Since not all of our input is Gaussian (i.e. some distributions are skewed) we use the data transformation Python package QuantileTransform from Scikit-learn (Pedregosa, et al., 2011), to

transform our inputs to a Gaussian distribution before conditioning on new measurements with *ccandu*. After the conditioning we inverse transform our outputs back.

An overview of the measurement locations and frequencies can be seen in Table 1 and Table 2, respectively. Furthermore, we defined three areas (Area 1, Area 2 and the Exclusion Zone) to compare our results, shown in Figure 3a. The measurement locations are indicated on the map of Rotorua in Figure 3b.

3.2.1 Scenario 1

The data collected in the monitoring scenarios are in the future in 2021-2041. The scenarios have differences in measurement location and frequency. Scenario 1 uses 9 existing monitoring wells to gather new temperature and pressure data, see Table 1. For modelling convenience, the future measurements are taken in the model block centres where the monitoring well is located. Scenario 1 is subdivided in 1A and 1B, where in 1A we measure every year in 2021-2041 and in 1B we measure every second year in 2021-2041, see Table 2. The comparison of 1A and 1B will show the impact of measurement frequency on our prediction uncertainty. Scenario 1 will be the cheapest option of the three scenarios, since the monitoring wells already exist.

3.2.2 Scenario 2

For Scenario 2 we chose 9 new measurement locations, see Table 1, by looking at high temperature and pressure regions of the model, which might have a positive impact on the prediction uncertainty. The measurement locations are reasonably shallow like most wells in Rotorua but vary more in depth than in Scenario 1. In this Scenario the measurements are taken every year in 2021-2041. Comparing the results of Scenario 1A and 2 will indicate if prediction uncertainty can be reduced more by choosing new measurements at 'clever' locations. Scenario 2 represents an intermediate cost scenario since new wells have to be drilled to gather the new data.

3.2.3 Scenario 3

Scenario 3 combines Scenario 1A and 2 to collect new temperature and pressure measurements from 18 different locations. The measurements in Scenario 3 are taken every year in 2021-2041. Scenario 3 represents a more expensive scenario since data have to be collected from existing wells as well as from the new wells, which would have to be drilled. The results of Scenario 3 will show how much further the prediction uncertainty can be reduced by taking measurements at all 18 locations combined.

Table 1: The measurement locations of Scenario 1 and 2, where Scenario 1 includes the nearby existing monitoring wells. Measurement locations of Scenario 1 are at the block centres of the nearby monitoring well for modelling convenience. The measurement locations of Scenario 3 are the locations of Scenario 1 and 2 combined.

Scenario 1				**Scenario 2**		
Easting	Northing	Elevation (mRL)	Nearby well	Easting	Northing	Elevation (mRL)
1885526	5770919	297.5	G11	1884514	5774509	282.5
1885042	5771680	292.5	G12	1884325	5773772	200.0
1885990	5772901	275.0	G13	1884282	5771196	160.0
1885102	5772746	287.5	G14	1885335	5771414	287.5
1884399	5774559	282.5	G2	1886243	5773473	260.0
1884356	5771983	160.0	M24	1885644	5774284	140.0
1886041	5773015	115.0	M25	1885419	5773153	115.0
1885149	5774092	220.0	M27	1884480	5772884	220.0
1884628	5774458	220.0	M28	1884783	5773570	275.0

Table 2: The measurement frequency of each scenario.

Scenarios	**Measurement plan**
1A	Measured every year in 2021-2041 at 9 locations, near existing monitoring wells.
1B	Measured every second year in 2021-2041 at 9 locations, near existing monitoring wells.
2	Measured every year in 2021-2041 at 9 new locations.
3	Measured every year in 2021-2041 at 18 locations (scenario 1A and 2 combined).

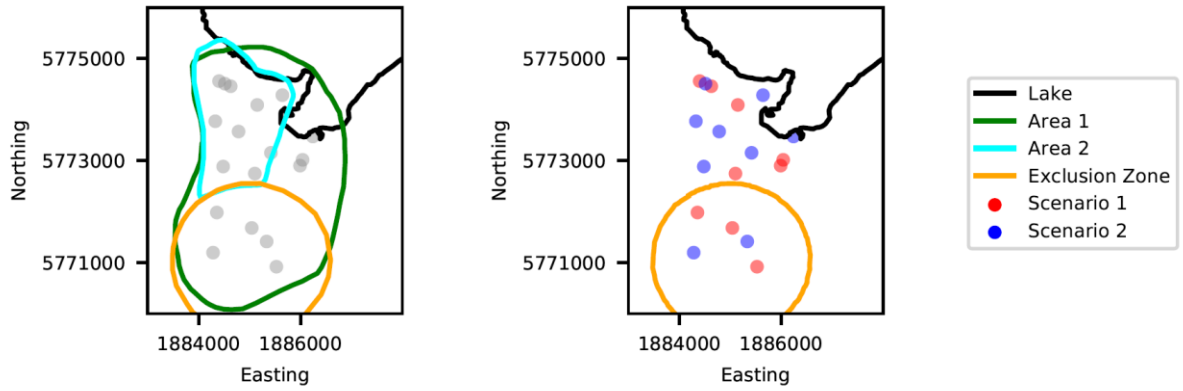

Figure 3: (a) Map of Rotorua showing the defined areas: Area 1, Area 2 and the Exclusion Zone. The outline of the lake is shown for reference. (b) Map of Rotorua with the monitoring locations of Scenario 1 and 2. The monitoring locations of Scenario 3 are the locations of Scenario 1 and 2 combined. The outline of the lake and the Exclusion Zone are indicated for reference.

4. RESULTS

The temperature, pressure and mass outflow predictions have been conditioned on the future temperature and pressure measurements of Scenario 1A, 1B, 2 and 3. The results presented in the figures and tables below are the QOI averaged over the areas (at different elevations) specified in Figure 3a.

The figures in this section show the predictions for each QOI in 2021-2041 at some elevations of the model (note: the temperature and pressure results at the surface are calculated in the middle of blocks, the surface mass outflow, however, is calculated at the top face of the blocks). The predictions include the calibrated model and a 95% confidence interval (the mean ± 2 standard deviations) of the original samples and the conditioned samples of each of the four scenarios. The tables in this section show the standard deviations of the QOI predictions in 2041 for specified areas and elevations to quantitatively show the impact of frequency, location and number of new measurements (note: the calibrated model predictions are not the mean of the original samples and the conditioned samples, the mean slightly varies).

4.1 Temperature predictions

The results from Figure 4, Figure 5, and Table 3 show that doubling the measurement frequency (Scenario 1A versus 1B) reduces the uncertainty (standard deviations) in most elevations and areas. We take the results of Area 1 as a representation of the overall model results, since this area encompasses all wells and all of the hot geothermal areas in the field. The percentages in Table 3 show the reduction in uncertainty of each scenario compared to the original (unconditioned) uncertainty. Measuring every year (Scenario 1A) compared to every second year (Scenario 1B) shows greater overall uncertainty reduction at the surface, -35% compared to -28%. At -900mRL Scenario 1B shows unexpectedly a marginally higher uncertainty reduction than Scenario 1A, -24% compared to -23%. The small difference in standard deviations could be due to a sampling error, since we take a relatively low number of samples (279) from the conditioned Gaussian. Choosing the new measurement locations (Scenario 2) in high temperature spots of the field achieves approximately the same overall uncertainty reduction compared to Scenario 1A. The results of Scenario 3 show the best uncertainty reduction throughout the reservoir. This is to be expected because this includes all 18 monitoring locations of Scenario 1 and 2, and the measurements are done every year.

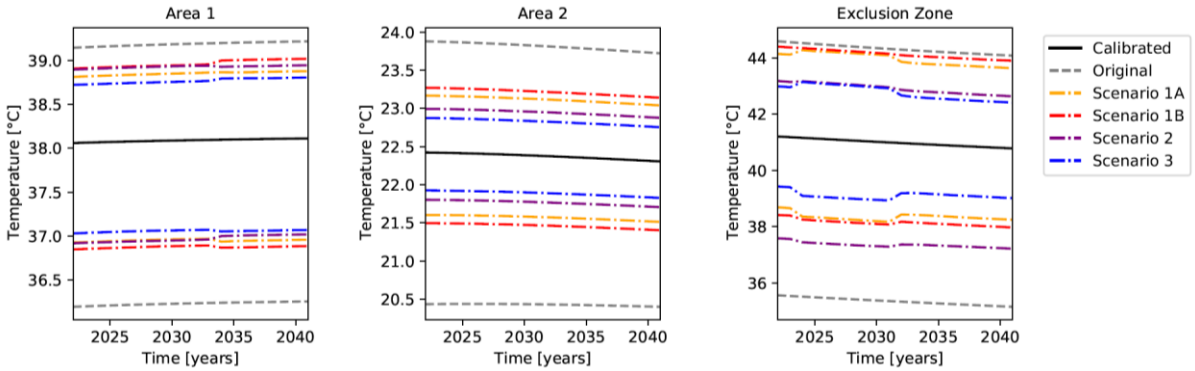

Figure 4: Impact of monitoring scenarios on temperature predictions for 2021-2041 at the surface for Area 1, Area 2 and the Exclusion Zone. The 95% confidence intervals of the original samples and of the samples for each scenario (equal to their mean ± 2 standard deviations).

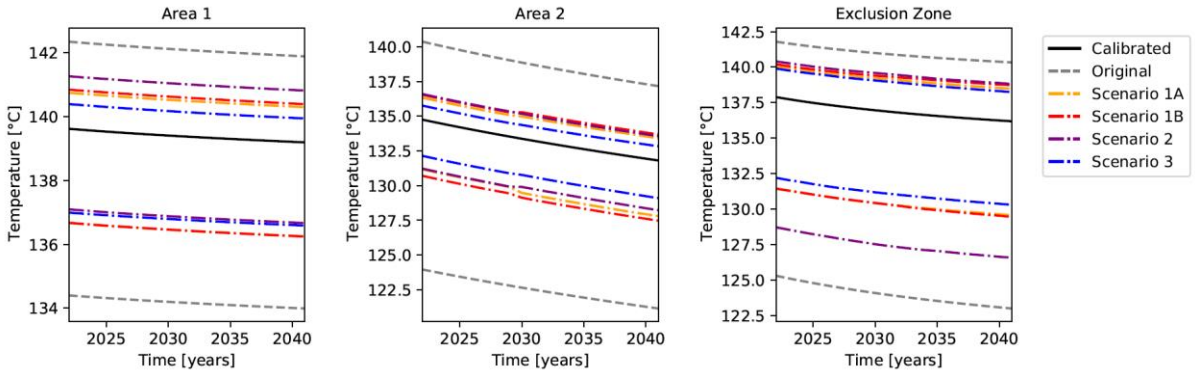

Figure 5: Impact of monitoring scenarios on temperature predictions for 2021-2041 at 200mRL for Area 1, Area 2 and the Exclusion Zone. The 95% confidence intervals of the original samples and samples of each scenario (equal to their mean ± 2 standard deviations).

Table 3: Temperature prediction uncertainty in 2041. The percentages show the difference between the standard deviations (std) of the scenarios compared to the standard deviations of the original (unconditioned) samples.

Elevation	Area	Calibrated temperature [°C]	Std original [°C]	Std Scenario 1A [°C]	Std Scenario 1B [°C]	Std Scenario 2 [°C]	Std Scenario 3 [°C]
Surface	Area 1	38.1	0.74	0.48 (-35%)	0.53 (-28%)	0.48 (-35%)	0.43 (-41%)
	Area 2	22.3	0.83	0.38 (-54%)	0.43 (-48%)	0.29 (-65%)	0.23 (-72%)
	Excl. Zone	40.8	2.23	1.34 (-40%)	1.48 (-34%)	1.35 (-39%)	0.84 (-62%)
200mRL	Area 1	139.2	1.97	1.01 (-49%)	1.04 (-47%)	1.04 (-47%)	0.84 (-58%)
	Area 2	131.8	4.00	1.40 (-65%)	1.55 (-61%)	1.33 (-67%)	0.93 (-77%)
	Excl. Zone	136.2	4.34	2.23 (-49%)	2.32 (-46%)	3.06 (-29%)	1.99 (-54%)
25mRL	Area 1	168.3	1.35	0.68 (-50%)	0.74 (-45%)	0.63 (-53%)	0.52 (-61%)
	Area 2	172.8	1.25	0.70 (-44%)	0.76 (-39%)	0.58 (-54%)	0.54 (-57%)
	Excl. Zone	178.8	2.00	1.17 (-42%)	1.17 (-41%)	0.84 (-58%)	0.77 (-62%)
-900mRL	Area 1	104.8	2.95	2.27 (-23%)	2.24 (-24%)	2.29 (-22%)	1.93 (-34%)
	Area 2	97.3	4.63	3.77 (-19%)	3.76 (-19%)	3.88 (-16%)	3.25 (-30%)
	Excl. Zone	75.8	4.99	4.61 (-7%)	4.52 (-9%)	4.41 (-11%)	3.83 (-23%)

4.2 Pressure predictions

The pressure predictions are presented in a similar way as the temperature predictions. Figure 6 and Figure 7 show the pressure uncertainty predictions in 2021-2041 at 200mRL and 25mRL, respectively. In contrast to the temperature uncertainty, the pressure uncertainty (standard deviation) is rather low. These results of low pressure uncertainty indicate that uncertain permeability, hot upflows and production have only little effect on pressure uncertainty. Applying a rock porosity uncertainty on the sample models might give more realistic pressure uncertainty results.

Comparing the pressure results of each scenario shows similar findings as the temperature results. In general, measuring every year (Scenario 1A) compared to every second year (Scenario 1B) improves the uncertainty reduction slightly more, with a maximum of 4% higher uncertainty reduction in Area 1 at -900mRL. Measuring at new locations (Scenario 2) improves the uncertainty at depth (25mRL and -900mRL) but is worse at and near the surface, compared to Scenario 1A. This could be explained by Scenario 2 having less monitoring locations near the surface and more at greater depth. Measuring at the 9 existing and 9 new monitoring locations (Scenario 3) shows the best uncertainty improvement, which is to be expected because it combines Scenario 1A and 2. However, this is also the most expensive monitoring plan of the proposed scenarios.

4.3 Mass outflow predictions

The mass outflow predictions at the surface are presented in Figure 8 and Table 5. It is worth noting that mass outflow is not measured for the monitoring scenarios. Nevertheless, the uncertainty of the mass outflow predictions is reduced when only temperature and pressure measurements are considered.

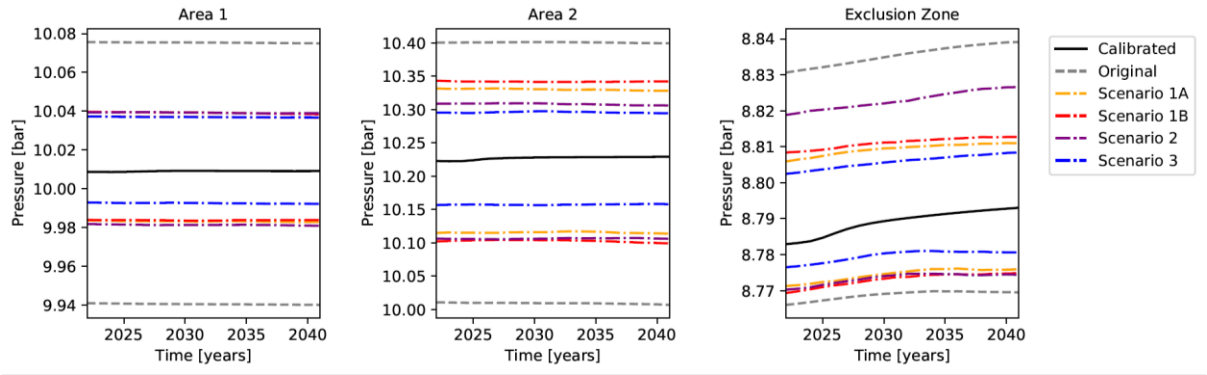

Figure 6: Impact of monitoring scenarios on pressure predictions for 2021-2041 at 200mRL for Area 1, Area 2 and the Exclusion Zone. The lines of the original samples and the conditioned samples (of each scenario) visualise a 95% confidence interval of the samples (equal to their mean ± 2 standard deviations).

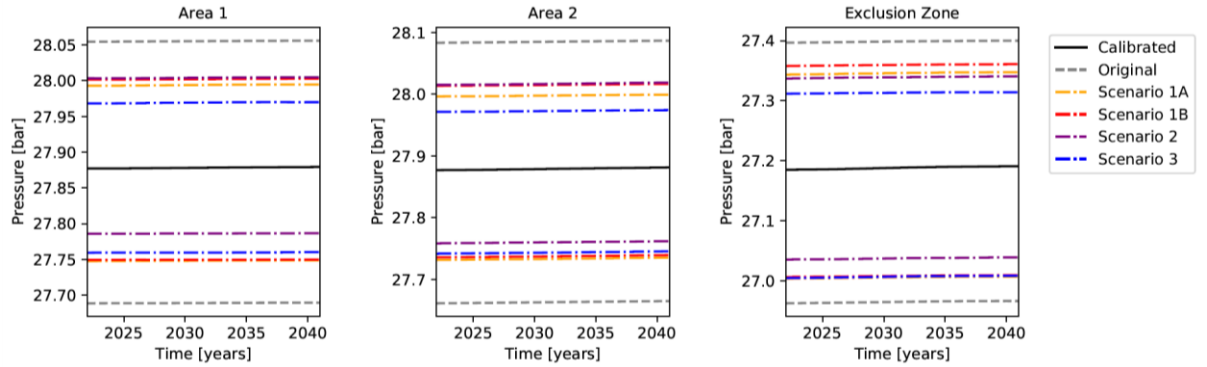

Figure 7: Impact of monitoring scenarios on pressure predictions for 2021-2041 at 25mRL for Area 1, Area 2 and the Exclusion Zone. The lines of the original samples and the conditioned samples (of each scenario) visualise a 95% confidence interval of the samples (equal to their mean ± 2 standard deviations).

Table 4: Pressure uncertainty results 2041. The percentages show the difference between the standard deviations (std) of the scenarios compared to the standard deviations of the original (unconditioned) samples.

Elevation	Area	Calibrated pressure [bar]	Std original [bar]	Std Scenario 1A [bar]	Std Scenario 1B [bar]	Std Scenario 2 [bar]	Std Scenario 3 [bar]
Surface	Area 1	1.38	0.00051	0.00037 (-28%)	0.00037 (-26%)	0.00041 (-20%)	0.00030 (-41%)
	Area 2	1.12	0.00149	0.00090 (-42%)	0.00087 (-44%)	0.00100 (-36%)	0.00077 (-50%)
	Excl. Zone	1.18	0.00228	0.00202 (-11%)	0.00194 (-15%)	0.00166 (-27%)	0.00146 (-36%)
200mRL	Area 1	10.0	0.034	0.013 (-60%)	0.014 (-60%)	0.015 (-57%)	0.011 (-67%)
	Area 2	10.2	0.098	0.054 (-45%)	0.061 (-38%)	0.050 (-49%)	0.034 (-65%)
	Excl. Zone	8.8	0.017	0.009 (-50%)	0.009 (-46%)	0.013 (-25%)	0.007 (-60%)
25mRL	Area 1	27.9	0.092	0.061 (-33%)	0.063 (-31%)	0.055 (-40%)	0.052 (-43%)
	Area 2	27.9	0.105	0.066 (-37%)	0.069 (-34%)	0.064 (-39%)	0.057 (-46%)
	Excl. Zone	27.2	0.108	0.085 (-21%)	0.088 (-19%)	0.075 (-30%)	0.076 (-30%)
-900mRL	Area 1	113.0	0.138	0.125 (-10%)	0.130 (-6%)	0.117 (-16%)	0.101 (-27%)
	Area 2	112.5	0.184	0.159 (-13%)	0.165 (-10%)	0.155 (-16%)	0.132 (-28%)
	Excl. Zone	112.5	0.198	0.172 (-13%)	0.181 (-9%)	0.170 (-14%)	0.149 (-25%)

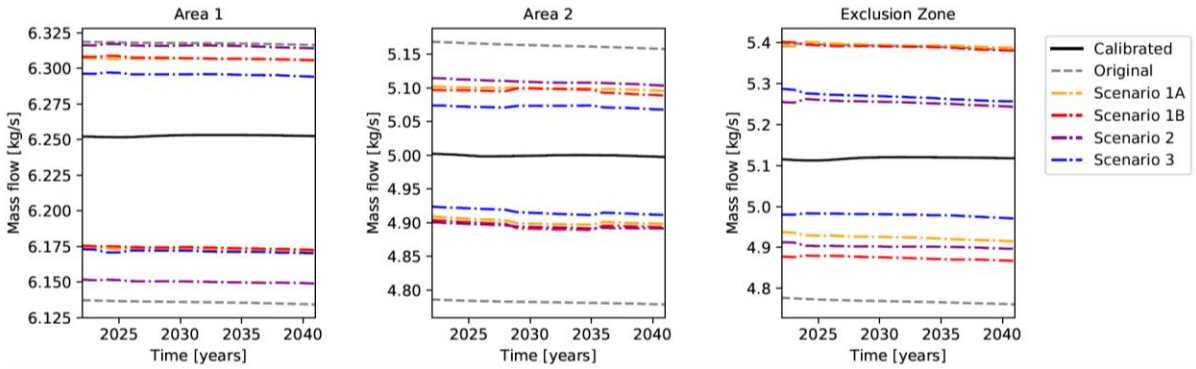

Figure 8: Impact of monitoring scenarios on mass outflow predictions for 2021-2041 at the surface for Area 1, Area 2 and the Exclusion Zone. The lines of the original samples and the conditioned samples (of each scenario) visualise a 95% confidence interval of the samples (equal to the mean ± 2 standard deviations).

Table 5: Mass outflow uncertainty results 2041. The percentages show the difference between the standard deviations (std) of the scenarios compared to the standard deviations of the original (unconditioned) samples.

Elevation	Area	Calibrated massflow [kg/s]	Std original [kg/s]	Std Scenario 1A [kg/s]	Std Scenario 1B [kg/s]	Std Scenario 2 [kg/s]	Std Scenario 3 [kg/s]
Surface	Area 1	6.25	0.046	0.033 (-27%)	0.033 (-27%)	0.041 (-9%)	0.031 (-32%)
	Area 2	5.00	0.095	0.049 (-48%)	0.049 (-48%)	0.053 (-44%)	0.039 (-59%)
	Excl. Zone	5.12	0.152	0.118 (-24%)	0.128 (-17%)	0.087 (-44%)	0.072 (-54%)

5. CONCLUSIONS & FUTURE RESEARCH

The results of the impact of each of the monitoring scenarios show that overall, the prediction uncertainty reduces slightly more when measurements are taken every year (Scenario 1A) instead of every second year (Scenario 1B). Since the uncertainty reduction in Scenario 1A compared to 1B is minor, measuring every year might not be worth the extra time and money. Taking measurements at new locations with high temperatures and pressures (Scenario 2) shows a similar impact on the prediction uncertainty, some areas and elevations are worse, and some are better than for Scenario 1A. Taking measurements at all 18 locations spread across the field (Scenario 3) shows the biggest improvement in the prediction uncertainty. Nevertheless, this is also the most expensive monitoring plan and might not be worth the money.

In this study, in Scenario 2, we attempted to choose the new measurement locations by looking at high temperature and pressure regions, which would hopefully result in a higher reduction of the prediction uncertainty. However, the reduction in prediction uncertainty of Scenario 2 was on average in the same ballpark as for Scenario 1A (existing measurement locations). Although the uncertainty reduction is on average the same, the results indicate that measuring at different locations improves the uncertainty reduction in different areas and elevations.

In this study we supplied a known set of measurements as a scenario to mimic a monitoring plan and compared different monitoring plans. To work out the best possible monitoring plan for reducing uncertainty, this could be formulated as an optimisation problem. One method is to compare the Data Worth impact of monitoring each individual block on the area of interest and choose a combination of blocks with the most significant impact. The drawback is that this method is very time consuming. Another method that is less time consuming would be to study the temperature and pressure uncertainty in each individual block and monitor a combination of the most uncertain blocks. The disadvantage of this method, however, is that blocks with high prediction uncertainty do not necessarily have the highest impact on the uncertainty reduction of an area of interest.

Lastly, in our results we discussed the economics of each scenario qualitatively. This could be improved on by introducing an economic cost factor for the comparison of the scenarios. In this study we investigate a couple of scenarios to investigate frequency, location and quantity of measurements. However, this is a tool for decision makers to design and compare monitoring plans in which they are interested. This framework is not limited to Rotorua or the quantities of interest explored here. It can be used on mature production geothermal fields for monitoring where quantities of interest could include future steam flow, surface feature predictions or future pressure trends. It can also potentially be used for resource assessment of new geothermal fields to find the best places to take measurements for quantifying the size of the geothermal field.

ACKNOWLEDGEMENTS

The authors wish to acknowledge the use of New Zealand eScience Infrastructure (NeSI) high performance computing facilities as part of this research. New Zealand's national facilities are provided by NeSI and funded jointly by NeSI's collaborator institutions and through the Ministry of Business, Innovation & Employment's Research Infrastructure programme. URL https://www.nesi.org.nz. The authors would also like thank Bay of Plenty Regional Council for the data they have provided over the years and the MBIE research programme "Empowering Geothermal" which has in part funded this research.

REFERENCES

Alexanderian, A. (2021). Optimal experimental design for infinite-dimensional Bayesian inverse problems governed by PDEs: a review. *Inverse Problems*.

Croucher, A., O'Sullivan, M., O'Sullivan, J., Yeh, A., Burnell, J., & Kissling, W. (2020). Waiwera: A parallel open-source geothermal flow simulator. *Computers & Geosciences*, 141, 104529.

Cui, T., Fox, C., & O'Sullivan, M. J. (2011). Bayesian calibration of a large-scale geothermal reservoir model by a new adaptive delayed acceptance Metropolis Hastings algorithm. *Water resources Research, 47*, (10).

Dekkers, K. (2021). *Inverse Modelling and Uncertainty Quantification of a Computational Model of Rotorua.* Eindhoven University of Technology.

Dekkers, K., van Vlijmen, M., O'Sullivan, J., Gravatt, M., Popineau, J., & O'Sullivan, M. (2020). An Updated Computer Model of the Rotorua Geothermal Field. Proc. *42nd New Zealand Geothermal Workshop.* Waitangi, New Zealand.

Environment Bay of Plenty (EBOP). (1999). *Rotorua Geothermal regional Plan.* Resource Planning Publication 99/02. Retrieved from Bay of Plenty Regional Council.

Finsterle, S. (2007) *iTOUGH2 User's Guide*, Report LBNL-40040, Earth Sciences Division Lawrence Berkeley National Laboratory, University of California, Berkeley, CA 94720, USA. 137 p.

Jiang, S., Sun, W., & Durlofsky, L. J. (2019). A data-space inversion procedure for well control optimization and closed-loop reservoir management. *Computational Geosciences*, 1-19.

Kaipio, J., & Somersalo, E. (2006). *Statistical and computational inverse problems* (Vol. 160). Springer Science & Business Media.

Maclaren, O. J., Nicholson, R., Bjarkason, E. K., O'Sullivan , J. P., & O'Sullivan, M. J. (2020). Incorporating Posterior-Informed Approximation Errors Into a Hierarchical Framework to Facilitate Out-of-the-Box MCMC Sampling for Geothermal Inverse Problems and Uncertainty Quantification. *Water Resources Research, 56*, e2018WR024240.

Modelling Uncertainty and Data Group UoA. (2021). ccandu: conditional composition and uncertainty (alpha version). *(Under development, alpha version available on request.)*.

NIWA, the University of Acukland, University of Otago, Manaaki Whenua - Land Research. (2021, 11 08). *New Zealand eScience Infrastructure*. Retrieved from https://www.nesi.org.nz/

Pedregosa, F., Varoquaux, G., Gramfort, A., Michel, V., Hirion, B., Grisel, O., . . . Duchesnay, E. (2011). Scikit-learn: Machine Learning in Python. pp. 2825-2830.

Pukelsheim, F. (2006). Optimal design of experiments. *Society for Indusstrial and Applied Mathematics*.

Ratouis, T. M., O'Sullivan, M. J., & O'Sullivan, J. P. (2016). A Numerical model of Rotorua Geothermal Field. *Geothermics*.

Sun, W., & Durlofsky, L. J. (2017). A new data-space inversion procedure for efficient uncertainty quantification in subsurface flow problems. *Mathematical Geosciences, 49*(6), 679-715.